SAND2008-7157C
09DEL-1055

Transient Liquid Penetration of Early-Injection Diesel Sprays

Lyle M. Pickett, Sanghoon Kook, Timothy C. Williams
Sandia National Laboratories

ABSTRACT

Diesel low-temperature combustion strategies often rely on early-injection timing to allow sufficient fuel-ambient mixing to avoid NO_x and soot-forming combustion. However, these early injection timings permit the spray to penetrate into a low ambient temperature and density environment where vaporization is poor and liquid impingement upon the cylinder liner and piston bowl are more likely to occur. The objective of this study is to measure the transient liquid and vapor penetration at early-injection conditions. High-speed Mie-scatter and shadowgraph imaging are employed in an optically accessible chamber with a free path of 100 mm prior to wall impingement and using a single-spray injector. The ambient temperature and density of the chamber are well-controlled (uniform) and varied according to expected early-injection timings. Injector parameters such as injection pressure, injection duration, nozzle size, multiple injections, and fuel distillation properties are also varied.

Results show that an injection duration less than one-half of the development time for a steady liquid length will produce liquid penetration distances that are less than that of a steady-state spray. Using multiple, short injections also limits the liquid penetration while permitting the vapor-phase to continue to penetrate into the chamber. Small nozzle diameters are helpful in limiting liquid penetration if sprays reach a steady-state liquid length. However, if the injection mass is kept constant, requiring a longer injection duration with small nozzles, the same maximum liquid penetration results as that of larger nozzles (provided injection durations are short enough such that liquid does not reach the steady-state liquid length). Similar findings are also obtained with injection pressure variation and the same injected mass: short injection durations at high injection pressure produce the same maximum liquid penetration as longer injection durations at low injection pressure. Fuel distillation property variation shows an expected benefit of shorter liquid penetration for low-boiling-point-temperature fuels.

INTRODUCTION

Low-temperature diesel combustion strategies have shown promise in reducing nitrogen oxide (NO_x) and particulate matter (PM) emissions. However, these combustion modes have also been shown to produce higher unburned hydrocarbon (UHC) and carbon monoxide (CO) emissions [1]. As a result, the combustion efficiency may decrease for low-temperature combustion (LTC) compared to traditional diesel combustion.

Researchers are working to understand the source of this inefficiency, hoping to minimize UHC and CO emissions while maintaining low PM and NO_x emissions. One potential source for UHC emissions is liquid fuel that wets in-cylinder surfaces. In contact with cooler, solid surfaces such as the piston bowl and cylinder liner, the liquid fuel film is less likely to vaporize and mix with the charge gas and burn effectively. Unfortunately, when using a low-volatility diesel fuel, liquid wall impingement is far more likely for LTC strategies, which often rely on injection timing well before top-dead center (TDC) (*e.g.,* [1-20]). This early-injection timing allows more time for fuel-ambient mixing prior to ignition and combustion, potentially avoiding fuel-rich, NO_x- and soot-forming

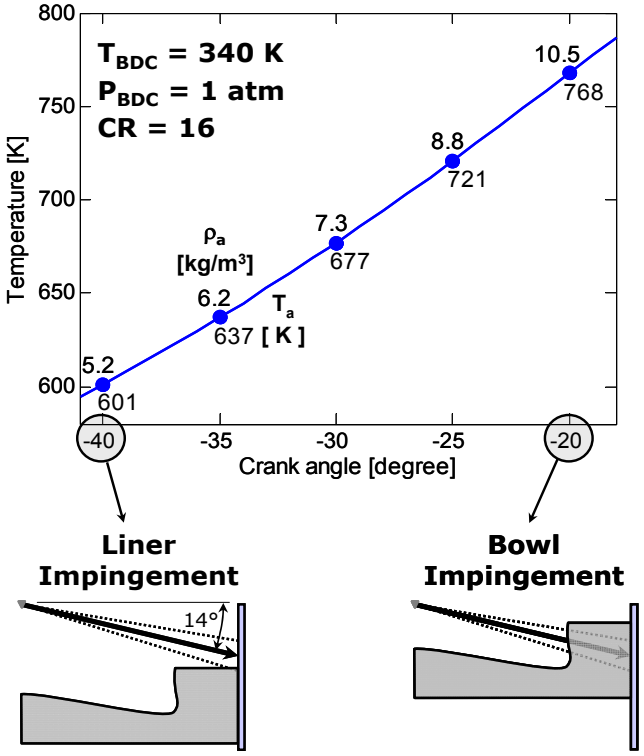

Figure 1. Computed in-cylinder charge ambient gas temperature T_a and density ρ_a at various crank-angle degrees during compression, assuming polytropic compression, γ = 1.35, compression ratio 16, and BDC conditions given. Schematics showing the piston position, and spray targeting for a 152° included-angle injector [4], are also shown.

combustion, but the spray enters into a low-density, low-temperature environment that offers little resistance to the liquid spray penetration. Figure 1 shows the charge-gas density and temperature typical for good-performance early-injection timings (*e.g.,* [7,10]), along with a schematic showing the spray targeting for a conventional diesel injector spray angle [4].

As indicated in the schematic, a diesel spray with a conventional, wide spray is likely to impact the cylinder liner with earlier injection timings. Indeed, optical visualization using a wide-angle injector confirms that liner impingement by liquid does occur with -40 crank-angle degree (CAD) injection timing relative to TDC [8]. Although not optically confirmed in other LTC test engines, fuel missing the bowl and possibly wetting the liner is suspected as a major source of high UHC, poor combustion efficiency, and problems such as oil dilution [5,9,13]. Conventional wide-angle injectors with timings of -30 to -20 CAD, still considered early compared to conventional diesel, also show liquid impingement upon the piston bowl, as confirmed by optical diagnostics [4,7].

To avoid liquid fuel impingement outside of the bowl, as well as to minimize the formation of liquid films within the bowl, researchers have attempted to use various narrow-angle injectors and bowl shapes for early-injection LTC [2,11-16]. Emissions and efficiency improvements have been noted for some low-load LTC operating conditions with narrow-angle injection, but there is difficulty utilizing available in-cylinder oxygen at high load [18] and performance and emissions suffer compared to conventional wide-angle injection [11]. In addition, although earlier injection timings may be used to keep fuel within the bowl, liquid films still form once fuel reaches the piston bowl [2,14-16]. In some cases, these liquid films burn as pool fires [15,16], which can be a source of soot and NO_x emissions [16], counter to the goal of early-injection LTC.

Mitigation of liquid impingement upon the piston bowl, and improved mixing to achieve more premixed LTC, can be promoted by use of specialized injectors with small nozzle size (*e.g.,* [10,16,17]), however, this injection system is not optimal for high-load conventional diesel combustion [17]. Alternatively, fuels that vaporize more easily than diesel have shown promise for premixed LTC (*e.g.,*, [19,20]), in part because liquid impingement is reduced (they also have different ignition characteristics). Other strategies utilize multiple injections as a method for limiting liquid penetration and preventing formation of fuel films [8,15].

The discussion above highlights the importance of understanding spray mixing and vaporization processes, for in-cylinder conditions and fuels that are applicable to early-injection LTC. Suitable diesel LTC performance can be expected only if obstacles surrounding liquid wall wetting can be overcome, while also achieving low-emissions, high-efficiency combustion.

TDC LIQUID-PHASE PENETRATION RESEARCH

One difficulty in the successful application of early-injection LTC is that little quantitative data exist for vaporizing sprays at ambient (charge-gas) conditions typical of early injection (*i.e.*, Fig. 1). Proposed injector hardware, or spray predictions of liquid penetration to prevent wall wetting, are therefore suspect. A simple reason for this deficiency, experimentally, is that liquid impinges upon in-cylinder surfaces, thus preventing further assessment of how far the liquid would have penetrated as a free spray. In contrast to early-injection conditions, there has been significant research about the governing processes that limit liquid penetration at traditional diesel conditions where fuel is injected near TDC [21-25].

Figure 2 shows spray liquid [21] and vapor [26] penetration results at conditions typical of past research (near-TDC injection), as well as injection at -20 CAD, an early-injection condition of more interest to this study. For both conditions, the rate of injection has a top-hat shape (bottom curve) and the injection duration is the same. With increasing time after the start of injection (ASI), the liquid and vapor phases of the spray penetrate together. The spray penetrates more slowly into a high density environment [26]. As hot gases are entrained into the spray, the liquid phase eventually reaches an axial position where the liquid is vaporized completely [21-25]. The vapor phase continues to penetrate downstream, but the liquid phase fluctuates about a mean "quasi-steady" position throughout the duration of injection, as indicated in the figure. This maximum liquid penetration distance is defined as the quasi-steady liquid length, or simply the liquid length [21].

Measurement and prediction of this quasi-steady liquid length has been the focus of significant research over a wide range of conditions [21-25]. A large part of this

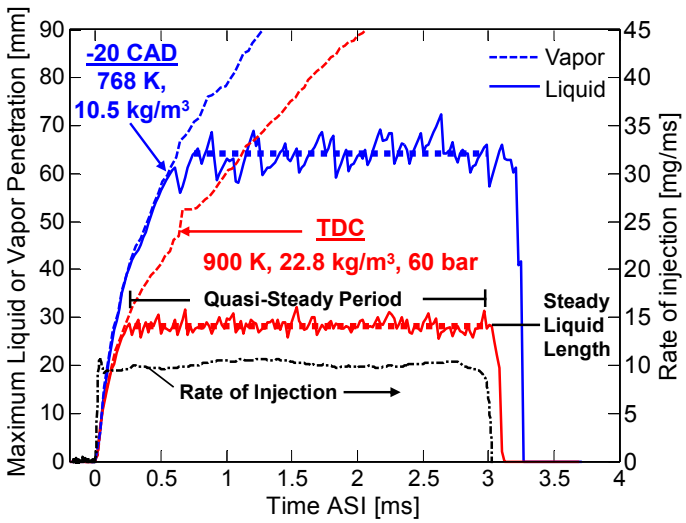

Figure 2. Measured vapor and liquid-phase axial penetration at near-TDC (red) and "early-injection" (blue) conditions. Rate of injection (black) at right axis. Ambient: 0% O_2 at temperature and density given. Injector: 0.185 mm diameter, KS1.5/86 nozzle, 110 MPa pressure, #2 diesel fuel. Data obtained in our facility.

Table 1. Parametric effects on quasi-steady liquid length.

Ambient temperature $T_a \uparrow$	Ambient density $\rho_a \uparrow$	Nozzle diameter $d \uparrow$	Injection pressure $P_{inj} \uparrow$	Fuel 90% boiling pt. $T_{90} \uparrow$
Liq. length: ↓	↓	↑	none	↑

dataset is available to download over the internet [27]. Table 1 summarizes the trends evident from the liquid length measurements. These trends are in agreement with the results from Fig. 2. An increased ambient temperature and density, typical of a TDC condition, tends to shorten liquid length. An increased nozzle diameter or fuel boiling point tends to increase liquid length [21,23] and injection pressure has no effect [21,24,25]. The reason for the specific parameter trend is discussed in detail in the cited references.

Siebers [22] has shown that the liquid length trends in Table 1 can be explained by assuming mixing-limited vaporization. To develop this model, Siebers used a model fuel spray [26] to calculate the amount of ambient gas entrained into the spray relative to the fuel mass flow rate, $\dot{m}_a(x)/\dot{m}_f(x)$:

$$\frac{\dot{m}_a(x)}{\dot{m}_f(x)} = \frac{1}{F/A} \propto \tilde{S} = x \cdot \sqrt{\frac{\rho_a}{\rho_f}} \frac{a \cdot \tan(\theta/2)}{\sqrt{C_a} \cdot d} \qquad (1)$$

where θ is the jet full spreading angle, x is axial distance from the injector, $\tilde{S}$ is the non-dimensional penetration distance, ρ_f is fuel density, and C_a is the orifice area contraction coefficient. Siebers then calculated the fuel-ambient ratio $(F/A)_{liq}$ by mass where the enthalpy change in the ambient gases matches the energy required to heat and vaporize the liquid fuel at the local liquid-vapor equilibrium temperature. $(F/A)_{liq}$ depends upon the ambient gas temperature and density, as well as the particular fuel properties and fuel temperature. The full equation to predict the steady liquid length (L) is:

$$L = \frac{b}{a} \cdot \sqrt{\frac{\rho_f}{\rho_a}} \cdot \frac{\sqrt{C_a} \cdot d}{\tan(\theta/2)} \sqrt{\left(\frac{2}{(F/A)_{liq}} + 1 \right)^2 - 1} \qquad (2)$$

where b and a are correlation constants with suggested values of 0.41 and 0.66*, respectively.

The predictions of this model agree well with measurements of the liquid length over a wide range of parameters given in Table 1. The model's success in predicting the liquid length, along with its independence of injection pressure, implies that diesel fuel vaporization is controlled by mixing, rather than atomization processes. However, the experimental data used for comparison with model predictions only went as low as 700 K, and Siebers notes that departures from model predictions tend to occur at low-temperature, low-density conditions.

* Siebers later corrected the coefficient a to have a value of 0.75 [26], which changes b to 0.47 in order to maintain the same b/a ratio.

As shown in Fig. 1, early-injection LTC conditions can have ambient temperatures of 600 K or lower, depending upon the injection timing. Further investigation of liquid penetration at these conditions is therefore warranted. In addition, the liquid length measurements and predictions are based almost entirely on the quasi-steady period of liquid penetration. For TDC conditions, this may be acceptable because the fuel spray quickly reaches a quasi-steady liquid length (*e.g.*, after only 0.2 ms in Fig. 2). However, for early-injection conditions (-20 CAD), Fig. 2 shows that substantially more time is required for the fuel spray to reach a steady liquid-length condition and, depending upon the in-cylinder geometry, a steady liquid length may not be obtained if liquid impinges upon the wall. Furthermore, given the problems associated with LTC operation at high-load conditions, the injector may close (short injection duration) prior to attainment of a steady liquid length. In this case, the quasi-steady liquid length may have no relevance to the actual liquid spray penetration. Therefore, it is important to understand the transients of liquid penetration and vaporization for early-injection conditions.

OBJECTIVE

Our objective is to study liquid-phase penetration at conditions typical of early-injection LTC, paying specific attention to the injection transients. For this study, we use a constant-volume chamber with optical access and a free path of 100 mm prior to wall impingement. The large dimension allows assessment of steady and transient liquid penetration that would be impossible within a typical engine geometry. The ambient temperature and density of the chamber are well-controlled (uniform) and varied according to expected early-injection timings, like those given in Fig. 1. Although the constant-volume chamber cannot mimic transient changes to ambient conditions, as would happen during compression in an engine, the data generated is useful in that each injection parameter effect is decoupled from the uncertainty associated with changing ambient conditions.

Specific measurements of liquid penetration included in this investigation are: (1) the quasi-steady liquid length at early-injection conditions, (2) the effect of nozzle diameter, injection pressure, and boost (ambient density), (3) the effect of short, transient injections of the same fuel mass, (4) the effect of multiple injections, and (5) the effect of fuel distillation properties, comparing diesel to a lighter, more-volatile, kerosene fuel.

EXPERIMENTAL APPARATUS

COMBUSTION VESSEL- A cubical-shaped combustion chamber, 108 mm on a side, was used for these experiments. The fuel injector is mounted at the center of a metal side-port such that the diesel spray is directed into the center of the chamber. Sapphire windows located in four other ports of the combustion vessel

Table 2. Injector nozzles and flow coefficients for this study.

Nom. dia. [mm]	*K* factor	C_d	C_a	P_{inj} [MPa]	Fuel Temperature [K]
0.094	1.5	0.85	1.0	110	373
0.108	1.5	0.91	0.96	110	373
0.185	1.5	0.88	0.96	110	373

permit line-of-sight and orthogonal optical access to the injected fuel jet. Further details about the combustion chamber geometry and operation may be found in [27].

The thermodynamic state of the ambient gases within the core of the vessel was varied to simulate different early-injection conditions like those shown in Fig. 1. To eliminate uncertainty associated with heat-release effects on liquid penetration, and for comparison with past steady liquid length research [21], the ambient gas within the vessel was prepared inert, containing 0% O_2, 89.7% N_2, 6.5% CO_2 and 3.8% H_2O [27]. A mixing fan is used to maintain the uniformity of the ambient gases within the vessel, but the velocities of the gases are low (<0.5 m/s) and do not noticeably affect the penetrating spray—the vessel is essentially quiescent.

INJECTION EQUIPMENT- A Bosch second-generation common-rail injector (CRIP 2.2) equipped with a single-spray, axial nozzle was used for this study. Nozzles of different hole diameter were included in the test matrix, and specifications for these nozzles are given in Table 2. The nozzles are all convergent ($K = (d_i - d_o)/10$), hydroground nozzles (KS1.5/86 specification by Bosch); mini-sac type with a sac volume of 0.12 mm^3. The discharge (C_d) and area contraction (C_a) coefficients for these nozzles were measured at the fuel injection pressure and temperature using a force sensor similar to Ref. [22]. The nozzle coefficients were determined from long-injection events, where the flow is relatively steady, as shown in Fig. 2. Rate of injection measurements were also performed using the force sensor, and cumulative mass measurements, for short- or multiple-injection events to be shown.

FUELS- The distillation properties for the #2 diesel and kerosene fuels used in this study are given in Fig. 3 and further properties are given in Table 3. Note that the fuel properties are given at room temperature, which is lower than the 100 °C fuel temperature used in the experiments. The 90% boiling point (T_{90}) is 75 °C higher for diesel compared to kerosene. The liquid penetration is therefore expected to be longer for diesel. For reference, the boiling point temperature of two single-component fuels, n-heptadecane (n-c17) and heptamethylnonane (HMN), are also indicated on Fig. 3. These single component fuels are close to the T_{90} of the real, multi-component fuels, and they will be used later to model the liquid penetration of diesel and kerosene. Siebers [22] found good prediction of #2 diesel liquid lengths when using n-c17 as a surrogate fuel.

Table 3. Diesel and kerosene fuel measured properties.

	kerosene	**#2 Diesel**
T_{10} [°C]	170	211
T_{90} [°C]	240	315
T_{100} [°C]	266	350
Cetane Index	39	47
Cetane Number	38	46
Low. Heat. Value [MJ/kg]	43.228	42.975
Density at 15°C [kg/m^3]	812	843
Aromatics Vol. %	11.0	27.0
H_2 mass %	13.9	13.28
Sulfur [ppm]	1	9
Kin. Visc. (-20°C) [mm^2/s]	4.465	-
Kin. Visc. (40°C) [mm^2/s]	~ 1.4 (est.)	2.35
Freeze Point [°C]	-57	-
Flash Point [°C]	47	73

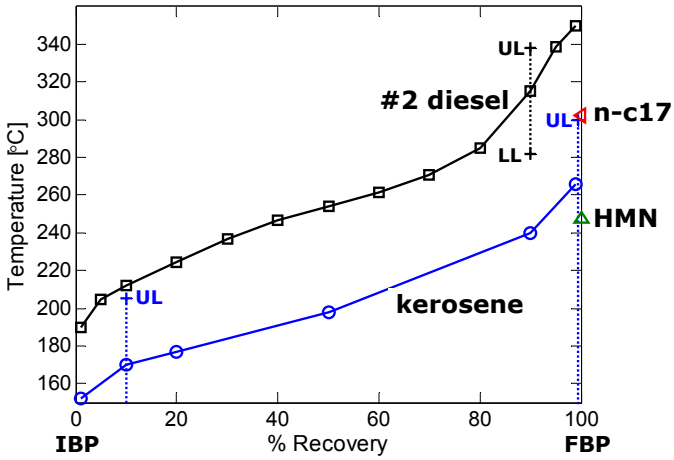

Figure 3. Distillation curves for #2 diesel and kerosene fuel samples used in this study. The atmospheric-pressure boiling points of single-component fuels n-heptadecane (n-c17) and heptamethylononane (HMN) are also given.

LIQUID AND VAPOR HIGH-SPEED IMAGING DIAGNOSTICS

Mie-scatter and shadowgraph imaging were performed simultaneously using high-speed imaging systems to track both the liquid-phase and vapor phases of the spray simultaneously. The results from Fig. 2 were obtained with these techniques. The ability to resolve the transients of a single injection sequence is especially important for sprays that do not attain a steady behavior, or, for example, if there are multiple injections where interaction between successive injections occurs. Also, the extent of fluctuation in liquid penetration, even at steady injection conditions, is important to understand the probability of liquid impingement upon in-cylinder surfaces. The average steady liquid length does not portray this information. For these reasons, results for single injections, rather than ensemble-averages, are shown in this paper.

MIE-SCATTER IMAGING- Scattered light from diesel spray liquid droplets was imaged using a high-speed

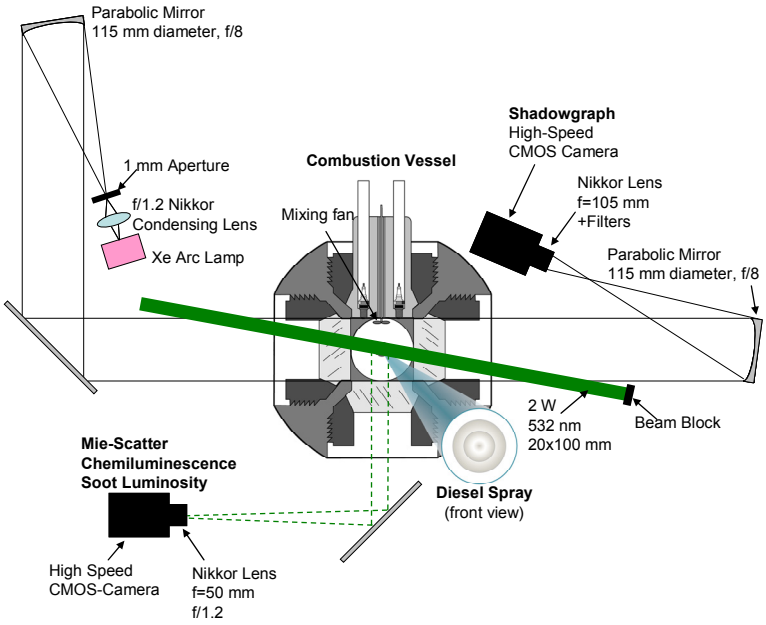

Figure 4. Combustion vessel and high-speed imaging setup. Mirror spacing not to scale.

CMOS camera and a continuous-wave laser. As shown in Fig. 4, a shadowgraph system was also operated simultaneously using a second high-speed CMOS camera. The time-resolved pair of shadowgraph and Mie-scatter images identifies the instantaneous position of both the vapor and liquid phases of the fuel spray.

The continuous-wave laser source was a frequency-doubled Nd:YAG laser (532 nm) operating with 2 W power. The laser was formed into a volume to illuminate only the liquid-phase region of the spray and also to avoid interference with the shadowgraph setup (Fig. 4). A volume illumination method, rather than a laser sheet, was utilized to ensure that all droplets spreading from the nozzle were illuminated to identify the maximum axial and radial distances of any liquid-phase fuel [21].

A high-speed CMOS camera, fitted with a 532-nm bandpass filter (10 nm FWHM) and a 50-mm focal length f/1.2 lens, was used to image Mie-scattered light at a near-right angle to the laser source. The bandpass filter was used to reject background thermal radiation from heated vessel walls. The camera was operated at reduced resolution (48 x 512 pixels) to allow fast framing periods (~20 μs) needed to capture dynamics of very fast diesel sprays. The lens was set to the maximum aperture (f/1.2) and the camera at maximum exposure duration (17 μs) to intentionally saturate the camera in the dense region of the spray while leaving sufficient dynamic range to identify regions of the spray where liquid completely evaporates. However, changes in laser power, exposure duration, or image threshold level (8/256 counts) did not significantly affect the measurable liquid penetration, similar to [21].

SHADOWGRAPH IMAGING- Shadowgraph and Schlieren imaging have been used for many years to identify refractive index gradients in various experiments [30]. For vaporizing diesel sprays, these techniques show the boundary between vaporized fuel and background ambient gases.

Figure 4 shows the lighting and imaging arrangement utilized to perform “focused” shadowgraph imaging. The setup and application is described in more detail in Ref. [31]. A 150-W (electrical power) mercury-xenon arc lamp with a small (1.7-mm) arc distance was used as a white light source. Light from the arc was filtered and collimated to pass through the combustion vessel. The collimated beam was then re-focused into a high-speed CMOS camera (Phantom v7.1) equipped with a Nikkor lens and a 532-nm 0°-incidence laser mirror, which acted to block Mie-scattered light from spray droplets.

As discussed in Ref. [31], a software routine was developed to detect the vapor boundary, based on differences between successive images and the gradient of a particular image. This method is needed to account for natural variations in refractive index of ambient background, caused by temperature non-uniformities within the boundary layer of the vessel. These non-uniformities of the ambient do not change significantly during injection, however, making detection of the vapor boundary more straightforward. Examples of vapor boundaries will be shown later, but the axial vapor penetration, already shown in Fig. 2, was the result of this method.

The shadowgraph (vapor boundary) images were also analyzed to determine the jet spreading angle. For consistency with Siebers′ method [22], images were time-averaged and analyzed in the region of the jet where liquid was also present, and the spreading angle was defined as the 50% threshold between the ambient and inner-spray intensity of the image (see Appendix A from [22]).

RESULTS AND DISCUSSION

The Results and Discussion is divided into four different sections. First, we present the steady-state liquid length at early-injection conditions for different nozzles and fuels. Next, we discuss the use of intake boost (turbocharging) as a method to limit the steady-state liquid penetration. Informed about the steady-state behavior, we then show how liquid penetration can be reduced from the steady-state liquid length by using short transient injections. We discuss the transient liquid penetration for nozzles and injection pressures with the same total mass injected. Finally, we show how multiple injections affect the transient liquid penetration.

STEADY-STATE LIQUID LENGTH AT EARLY-INJECTION CONDITIONS- As mentioned previously, there is little steady-state liquid length data at early-injection conditions because wall impingement occurs within typical engine geometries. To begin this study, we therefore examined long injection durations within the 100-mm combustion vessel. The ambient gas temperature and density were varied according to a

certain crank-angle degree during compression. Consider the temperature and density plotted in Fig. 1, which are for a BDC temperature of 340 K, and pressure of 1 bar. Obviously, many different BDC conditions exist, but 340 K is reasonable when considering heat transfer from the head, as well as internal and external EGR addition. The effect of boost, which changes the BDC pressure, and ultimately, the ambient density, will be considered in the next section.

Figure 5 shows the transient liquid penetration, and steady liquid length, for a relatively small nozzle (0.108 mm) and #2 diesel fuel. The maximum liquid penetration is shown for ambient conditions associated with CAD that were given in Fig. 1. As expected, the maximum liquid penetration decreases with CAD closer to TDC. Note that these CAD do not necessarily signify the exact timing of injection for which wall interaction will occur, because the penetrating spray takes a certain amount of time to reach its quasi-steady distance. For example, a 1-ms development time, which is 10 CAD at 1800 rpm, is representative of the time required to penetrate to the wall of the chamber or reach a steady liquid length. Therefore, the steady liquid lengths shown in Fig. 5 could be representative of final liquid length for an injection that started 10 CAD earlier than the CAD listed in Fig. 5. Conversely, if injection is started at the CAD listed in Fig. 5, the steady liquid lengths shown would be an overestimate of the final liquid penetration because of engine compression during the spray development.

In actuality, the time ASI to attain a steady liquid length increases as equivalent CAD timing is advanced. Although sprays penetrate more quickly at early CAD, because of the lower ambient density [26], the final liquid length is longer and the spray ultimately takes more time to reach this steady liquid penetration state. For example, the time to achieve steady liquid penetration approximately doubles, when comparing -20 CAD to -35 CAD. In later sections we will show that this increased time to attain steady liquid penetration can be important to the final liquid penetration, if injection duration is shortened during this period.

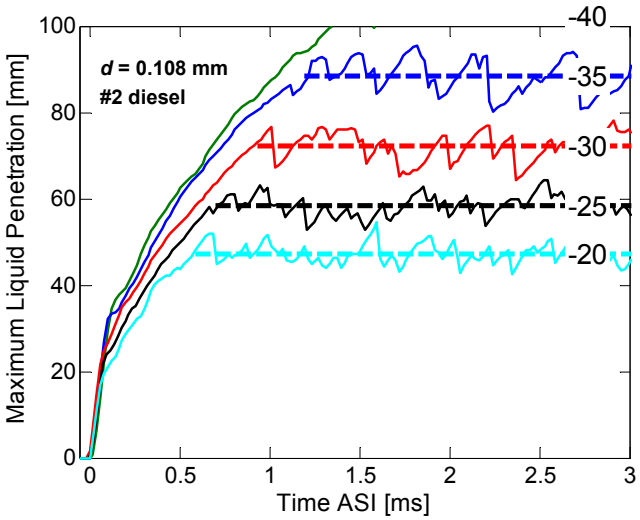

Figure 5. Liquid penetration histories at simulated ambient conditions corresponding to CAD from Fig. 1. Injector is 0.108 mm nozzle, 110 MPa, #2 diesel, with long injection duration. Single-injection results are shown, rather than ensemble-averages, to illustrate the extent of instantaneous liquid penetration and the transition to "steady" penetration.

Despite the use of a small nozzle, Fig. 5 shows that the steady liquid length is quite long relative to typical cylinder-liner or piston bowl radii, particularly for a light-duty engine for which small nozzles are more typical (*e.g.*, liner radius 40 mm, bowl radius 20 mm). In fact, liquid penetrates all of the way to the wall (100 mm) of the vessel at -40 CAD simulated conditions. These results confirm the difficulty of implementing early-injection diesel LTC without wall wetting.

Figure 6 shows transient liquid penetration at the same ambient conditions of Fig. 5, while changing the fuel to kerosene and increasing the nozzle diameter to 0.185 mm. Recall that an increase in nozzle diameter is expected to linearly increase the liquid length while a lower boiling point temperature of the fuel is expected to decrease the liquid length ([21-22] and Eq. (2)). The trends with respect to injection timing that were shown previously are repeated in Fig. 6, as the liquid length, and time to reach the steady liquid length, both increase with earlier CAD timing. The liquid lengths using kerosene and a larger nozzle diameter are approximately the same as Fig. 5, or even lower. For example, liquid wall impingement (>100 mm) occurs at conditions representing -40 CAD in Fig. 5, but there is no liquid impingement at -40 CAD conditions in Fig. 6. Therefore, the use of a low-boiling-point fuel (kerosene) more than compensates for the larger nozzle diameter to decrease the liquid length.

A direct comparison of the liquid and vapor penetration histories between kerosene and #2 diesel fuel is shown in Fig. 7 for the -20 CAD condition, now using identical

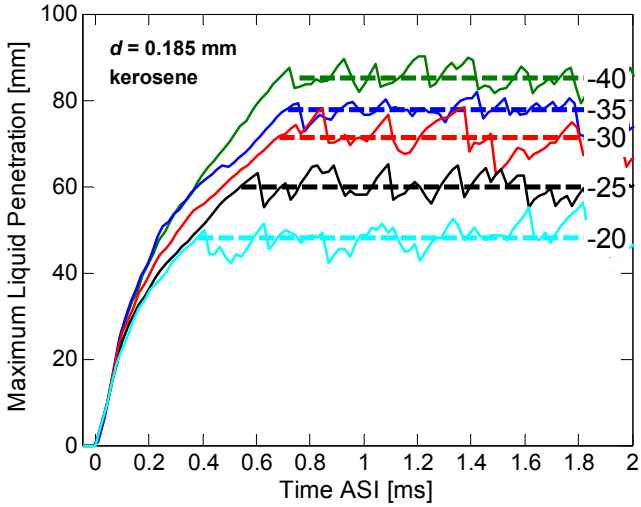

Figure 6. Liquid penetration histories using kerosene fuel and larger nozzle. Injector is 0.185 mm nozzle, 110 MPa, kerosene, with long injection duration. Compare to Fig. 5.

injector parameters. The steady liquid length is approximately 33% lower for kerosene compared to diesel at this condition. In addition, the time ASI to reach a quasi-steady liquid length is approximately 60% longer for diesel compared to kerosene. Despite the differences in the liquid-phase penetration history, there are no major differences in the vapor-phase penetration for the two fuels. The similarity in vapor penetration can be expected because the fuel injector pressure and nozzle size are identical, thereby imparting similar momentum to the fuel spray. The ambient density is also identical. As momentum exchange between the ambient and fuel spray slows the penetrating spray, a comparable vapor penetration for the two fuels is therefore expected [26].

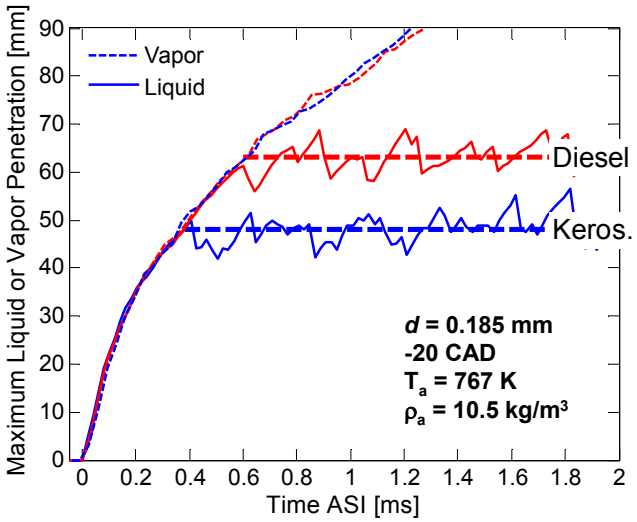

Figure 7. Comparison of liquid penetration histories for #2 diesel and kerosene fuel at -20 CAD simulated condition. Injector is 0.185 mm nozzle, 110 MPa, long injection duration.

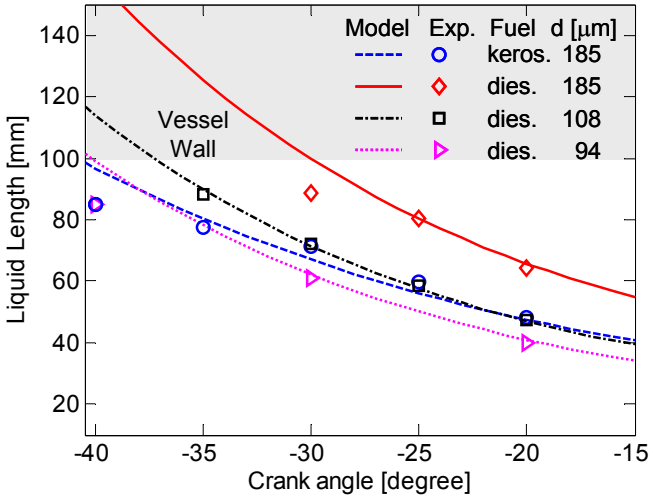

Figure 8. Steady-state liquid length measurements (symbols) and comparison to Siebers [22] model predictions (lines). Fuel impingement was measured at the vessel wall at 100 mm from injector for datasets with no symbols visible at -35 CAD or -40 CAD. Model inputs: heptamethylnonane as a surrogate for kerosene; n-heptadecane as a surrogate for diesel [22]; 12.3° as measured full spreading angle for 0.185 mm nozzle; 10.1° as measured full spreading angle for 0.108 mm and 0.094 nozzles. Spreading angles defined the same way as Ref. [22].

On the other hand, the liquid-phase "detaches" from the vapor head of the jet at different distances from the injector, corresponding to different amounts of entrained, hot ambient gases. For #2 diesel, the amount of entrained gas must necessarily be higher, to (1) reach higher mixture temperatures, and to (2) become more fuel-lean, as required to vaporize the fuel. Meanwhile, the time ASI to reach this mixture state must be higher because the overall penetration rate of diesel is the same as that of kerosene. The differences in liquid penetration transients between #2 diesel and kerosene may therefore be important, for example, if injection ends before the liquid-phase detaches. We will discuss this point later.

A summary of the measured steady liquid length distance for variations in fuel, nozzle size, and CAD is shown in Fig. 8. Along with the measurements (symbols), modeled liquid lengths are shown as connected lines. The modeled liquid lengths were calculated using Eq. (2), which is Siebers' model based on mixing-limited vaporization at a given ambient gas temperature and density [22]. Measured spreading angles from the shadowgraph imaging were used as inputs. Fuel properties for heptamethylnonane were used as a surrogate for kerosene, and n-heptadecane, for #2 diesel. Recall that the boiling point temperature of these single-component fuels is close to the 90% point of the distillation curve, T_{90} (Fig. 3), and choosing fuel surrogates based on T_{90} has been used successfully in the past for liquid-length prediction [22].

Figure 8 shows that the model predictions agree well with the measurements at -20 CAD, but are too high for earlier CAD near -40 CAD. Previously, Siebers also found that the model overpredicted liquid lengths at low-temperature, low-density conditions [22], which is the same tendency in this early-injection study. Note that when using #2 diesel, liquid impingement upon the vessel wall was observed at -40 CAD or -35 CAD for the 0.185 mm nozzle, and at -40 CAD for the 0.108 mm nozzle. These experimental data points are therefore not shown. However, the experimental data point prior to wall impingement also shows a trend of being lower than the model prediction. Despite this inaccuracy prior to wall impingement, the model provides expectations about the liquid length in a region where no measurements can be made, past the wall.

Regarding the effect of fuel type on liquid length, both the experimental measurements and model predictions show that #2 diesel liquid lengths increase more quickly with earlier injection than that of kerosene. For example, at -20 CAD the kerosene, 0.185-mm liquid length is essentially the same as the diesel, 0.108-mm liquid length. But the datasets, and model predictions, diverge with earlier injection timing. As mentioned above, the diesel, 0.108-mm condition experiences wall impingement at -40 CAD, but the kerosene liquid length

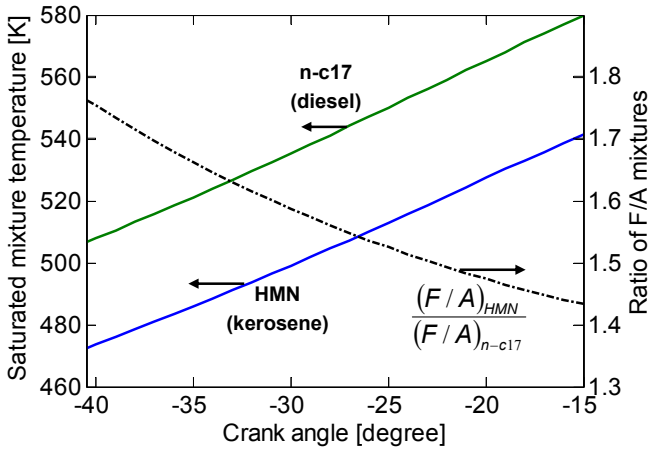

Figure 9. Saturated mixture temperature (left) and ratio of F/A mixture (right) predicted at the liquid length for surrogates n-c17 (for diesel) and HMN (for kerosene).

is lower (85 mm), and measureable. These results show that even if modifications are made to the injector to reduce the liquid length, such as reducing nozzle size to have the same liquid length, a fuel with a lower boiling point will still yield lower liquid lengths over a wider range of early-injection conditions.

Figure 9 explains what causes this fuel effect on liquid length at early-injection conditions. Model predictions of the mixture temperature at the liquid length, the saturated temperature at which fuel is entirely vaporized when mixed with the ambient at equilibrium, are plotted versus CAD. The right axis shows the predicted fuel-to-ambient ratio, $(F/A)_{liq}$, at the liquid length for kerosene, normalized by $(F/A)_{liq}$ for diesel, as represented by the fuel surrogates heptamethylononane and n-dodecane. As expected, the saturated temperature is lower, and the $(F/A)_{liq}$ higher, for kerosene compared to diesel. These two effects clarify how kerosene vaporizes more quickly compared to diesel within a given spray. But the reason that kerosene liquid lengths increase less than diesel during timing advancement is explained by the normalized *F/A* ratio. Figure 9 shows that kerosene actually becomes increasingly fuel-rich at the liquid length compared to diesel. By tolerating comparatively more fuel-rich mixtures at earlier CAD, the increase in liquid length is less for kerosene compared to diesel. One can recognize this effect on liquid length by referring to Eq. (2).

INTAKE PRESSURE EFFECTS ON QUASI-STEADY LIQUID LENGTH- With injector design and fuel chosen beforehand, what else can be done during a drive cycle to control the liquid length at early injection conditions? In this section, we discuss the effects of intake pressure (or boost). As was shown in Table 1, increasing ambient gas density (effectively pressure) is known to decrease quasi-steady liquid lengths. However, the effectiveness of increased boost on liquid length has not been explored at early-injection conditions.

Figures 10 and 11 show the effect of increased ambient gas density on the development of quasi-steady liquid lengths. Results are shown at simulated ambient conditions representing -40 CAD and -20 CAD, respectively. For these simulations, we make the assumption that the BDC temperature remains constant, which means that the ambient temperature at a given CAD (see Fig. 1) does not vary with ambient density. Therefore, only the ambient density changes when attempting to represent the effect of intake pressure boost. Transient liquid penetration measurements are shown using the same injector and injection pressure, but with different fuels. For the -40 CAD condition, recall that liquid impingement occurred upon the vessel wall when using diesel fuel. Consequently, kerosene fuel results are given for the -40 CAD condition (Fig. 10).

Consistent with Table 1, the quasi-steady liquid length decreases significantly with increasing ambient density,

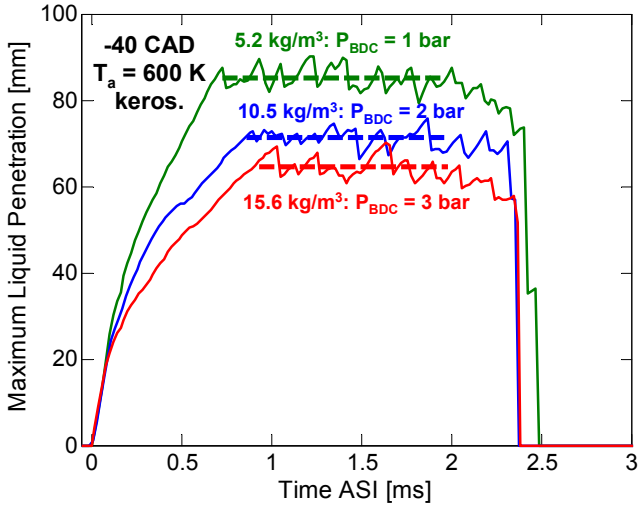

Figure 10. Effect of intake boost on quasi-steady liquid length. Ambient temperature is constant at 600 K, simulating -40 CAD with same BDC temperature (340 K). Injector is 0.185 mm nozzle, 110 MPa, kerosene fuel.

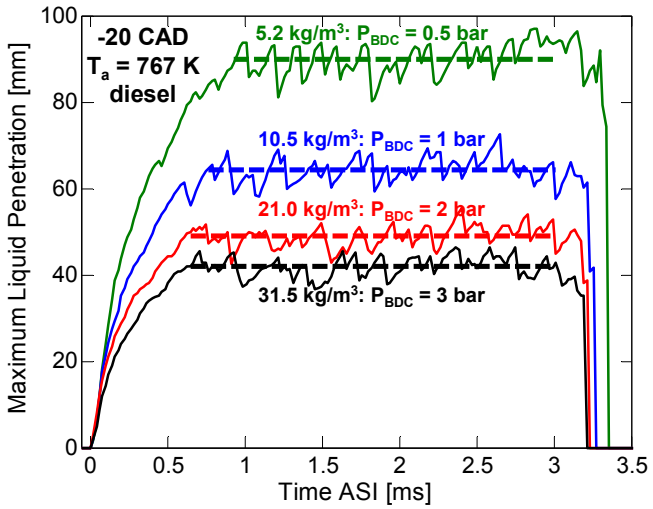

Figure 11. Effect of intake boost on quasi-steady liquid length at -20 CAD simulation. Other conditions the same as Fig. 10, except fuel is diesel.

which could possibly prevent liquid wall impingement at these early-injection conditions. The liquid length decrease with ambient density is related to two competing effects. First, Equation 1 shows that ambient entrainment increases in proportion to $\rho_a^{0.5}$, providing more energy to vaporize fuel at a given axial position. On the other hand, increased gas pressure (or density) raises the boiling point temperature of a fuel-ambient mixture, requiring increased mixing (lower $(F/A)_{liq}$) to vaporize the fuel [22]. In the end, the increased mixing with the ambient dominates to decrease the liquid length with increasing ambient density (see Eq. (2)).

These two competing effects do play a role, however, in determining the time required for the fuel spray to reach a quasi-steady liquid length. Fig. 10 shows that increasing the ambient density causes an increase in time ASI to achieve steady conditions, while Fig. 11 shows the opposite behavior. This apparently contradictory behavior can be explained by examining the change in $(F/A)_{liq}$ required to vaporize the fuel at the ambient temperature (CAD) of each figure.

Before providing this explanation, we first discuss the expectation for mixing times with respect to ambient density. Naber and Siebers [26] show that a non-dimensional penetration time ($\tilde{t}$) for a spray can be related to the non-dimensional penetration distance ($\tilde{S}$) as:

$$\tilde{t} = \frac{\tilde{S}}{2} + \frac{\tilde{S}}{4}\cdot\sqrt{1+16\cdot\tilde{S}^2} + \frac{1}{16}\cdot\ln\left(4\cdot\tilde{S}+\sqrt{1+16\cdot\tilde{S}^2}\right) \qquad (3)$$

and

$$\tilde{t} = t\cdot\sqrt{\frac{\rho_a}{\rho_f}}\frac{\tan(\alpha/2)}{\sqrt{C_a}\cdot d}\cdot U_f \qquad (4)$$

where, t is time, and U_f is the exit spray velocity. In the far-field limit of a spray, Eq. (3) has an $\tilde{S} = \tilde{t}^{0.5}$ dependency [26].

Equations (1)-(4) are then used to predict the expected mixing time (t_{ss}) to achieve a steady-state liquid length (L) where L now becomes the penetration distance x in Eq. (1). Proportionality relationships from these equations show that:

$$t_{ss} \propto \frac{L}{U_f}\cdot\frac{1}{(F/A)_{liq}} \quad . \qquad (5)$$

Since the predicted L depends upon $(F/A)_{liq}$, as well as ambient density, the change in t_{ss} when ambient density is varied is taken into account.

Equation (5) shows that the mixing times ASI to reach the liquid length may increase or decrease depending upon whether changes in L or $(F/A)_{liq}$ are dominant. Predicted values of t_{ss} are shown in Fig. 12 for the conditions of both Fig. 10 (-40 CAD) and Fig. 11 (-20 CAD). For reference, $(F/A)_{liq}$ is labeled near each data point on the figure.

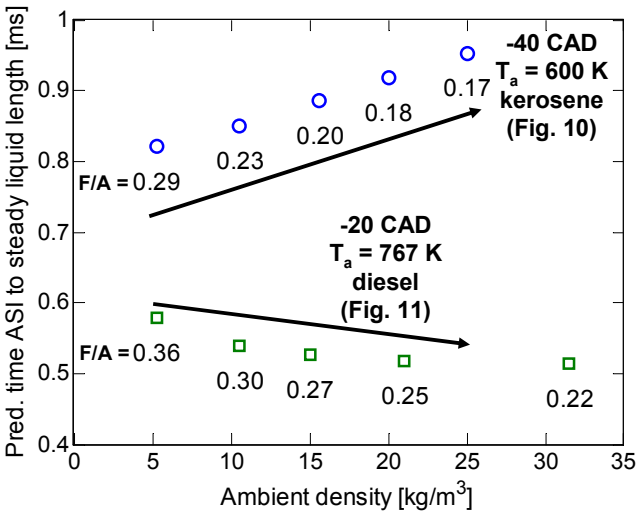

Figure 12. Predicted time for sprays to achieve a steady liquid length with respect to ambient density, for the conditions of Fig. 10 and Fig. 11. Time is calculated using the modeled liquid length and Eqs. (1)-(4). Although spreading angles may vary with ambient density [22], a constant full spreading angle of 12.3° is used for this calculation. The predicted F/A mixture at vaporization is also shown.

While $(F/A)_{liq}$ decreases with increasing ambient density for both CAD timings, requiring increased mixing within the jet, the predicted time to reach a steady liquid length has an opposite trend, depending upon the conditions (*i.e.,* ambient temperature). At 767 K (-20 CAD), the decreasing $(F/A)_{liq}$ effect, which requires extra mixing time, does not overtake the $t \propto \rho_a^{-0.5}$ effect from Eq. (4), and the t_{ss} decreases with increasing ambient density. In other words, decreasing L with increasing ambient density is dominant in Eq. (5). However, at 600 K (-40 CAD) with kerosene, the reverse is true as the decreasing $(F/A)_{liq}$ is dominant. Although not shown, diesel fuel has the same trend at 600 K. Both of these trends are in agreement with the experimental results shown by the direction of the arrows in Fig. 12. The predicted time ASI to achieve a steady liquid length is also in reasonable agreement with the experiment.

The experiments demonstrate that intake boost can have a beneficial effect in reducing liquid length. At earlier CAD (-40), boost can also delay the time to reach a steady liquid length. In an engine, this extra time can have an additional benefit in reducing wall-wetting, since compression will heat the ambient gas during this time, reducing the liquid length even further because of the hotter entrained ambient gas. However, at later CAD (-20), the competition between mixing time and F/A reduction reverses this trend, creating t_{ss} that are lower at high boost. These tradeoffs reinforce that it is important to consider the transients in spray development at early-injection conditions.

SHORT INJECTION DURATIONS TO LIMIT LIQUID PENETRATION- The results above have shown that the

time ASI (t_{ss}) to achieve a steady-state liquid length depends upon many parameters, including ambient temperature, ambient density, injector nozzle size, injection pressure (not shown, but obvious), and fuel. This time can be particularly significant at early-injection conditions, because the liquid lengths are quite long. In this section, we explore how ending injection prior to t_{ss} affects liquid penetration.

Relationship between Liquid and Vapor Penetration- Figure 13 shows high-speed imaging of the liquid and vapor, comparing a short, 0.35-ms injection to a steady, long injection. Several sets of images are given. Mie-scatter images are shown at the left at conditions representative of -40 CAD. The very top image is the liquid scatter during a long injection, while those below are for the 0.35-ms injection. The liquid boundary, shown in blue, is overlaid on shadowgraph images at the same timing in the middle. At the right, are shadowgraph images and liquid borders at -20 CAD conditions. The vapor and liquid penetration distances, as well as rate of injection, are plotted in Fig. 14.

The top, steady image shows that liquid penetrates all of the way across the chamber at the -40 CAD condition, which is confirmed by the liquid penetration curve for the long injection in Fig. 14. The need to limit liquid penetration for this condition is therefore apparent. The Mie-scatter images for the 0.35-ms injection show strong signal during injection at 0.2 ms ASI. After the end of injection (AEI), the liquid border moves downstream of the injector. The intensity of the scattered light begins to decrease significantly by about 0.6 ms. The liquid border also begins to shrink towards the jet center as the liquid is vaporized.

Comparison with the shadowgraph images (middle) shows that the liquid region penetrates at the head of the jet along with the vapor initially. As liquid evaporates AEI, the last liquid to vaporize is found at the head of the jet, but fuel vapor remains near the injector and at the jet edges. The liquid vaporizes completely at about 0.9 ms ASI (or 0.6 ms AEI) and reaches a maximum penetration distance from the injector of about 75 mm. Although liquid-phase fuel is no longer present, the vapor jet continues to penetrate downstream.

For this -40 CAD condition, Fig. 14 shows that the liquid and vapor penetration rate for the 0.35-ms injection is initially the same as that of the long injection duration. However, the penetration rate slows from that of the long injection at about 0.6 ms, approximately double the time ASI that the injection rate begins to ramp down. Afterwards, the liquid phase stalls and vaporizes at about 75 mm from the injector, as was shown in the imaging. The vapor phase continues to penetrate and

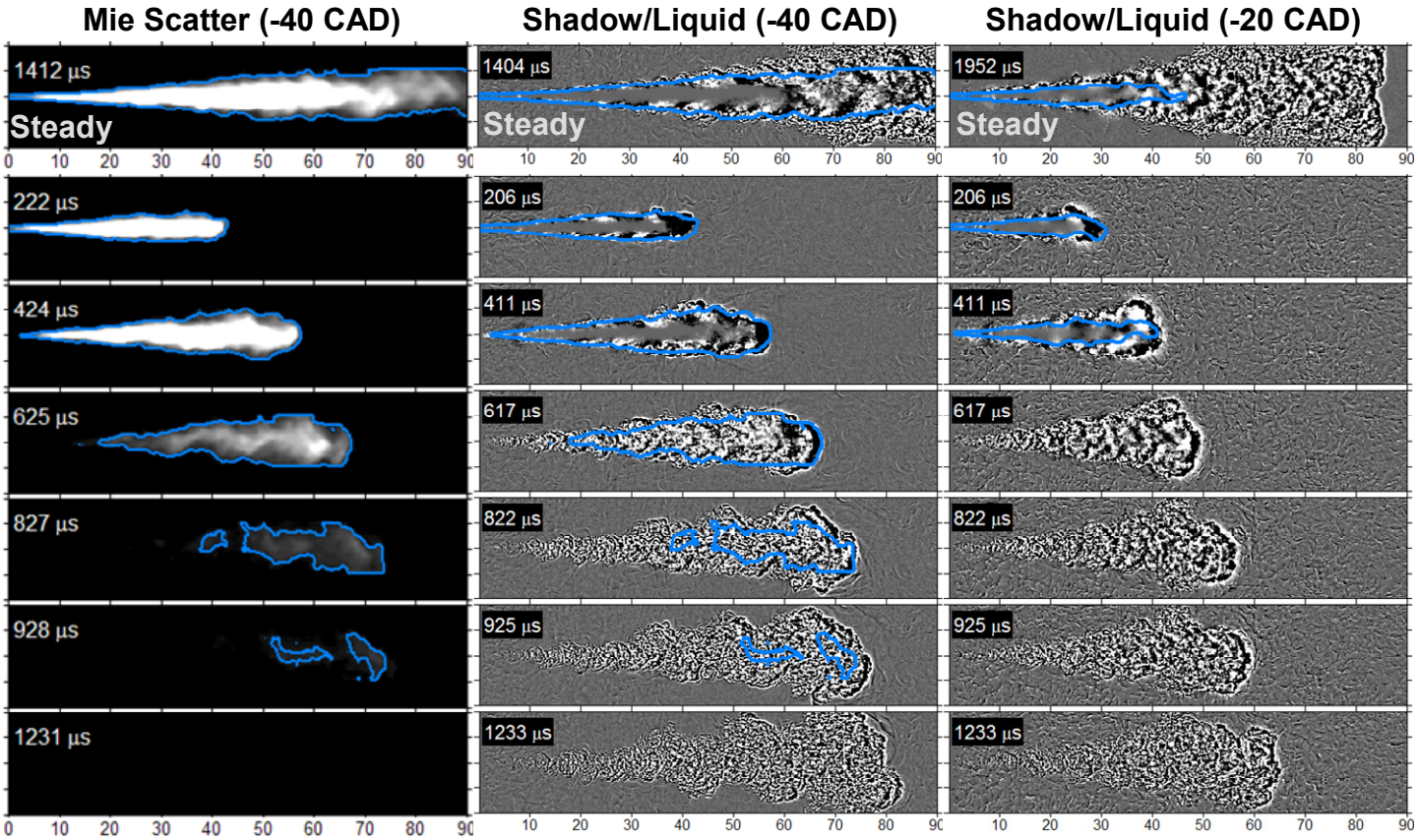

Figure 13. Mie-scatter and shadowgraph imaging showing the effect of short injection durations on liquid and vapor penetration. Top image row is for steady conditions for comparison. (Left) Mie-scatter liquid imaging at -40 CAD conditions. (Middle) Shadowgraph images with liquid boundary overlaid at -40 CAD conditions. (Right) Shadowgraph/liquid images at -20 CAD conditions. Injector conditions: 0.108 mm nozzle, 110 MPa, #2 diesel, 1.2 mg injected in 0.35 ms. Image scale in mm (from the injector).

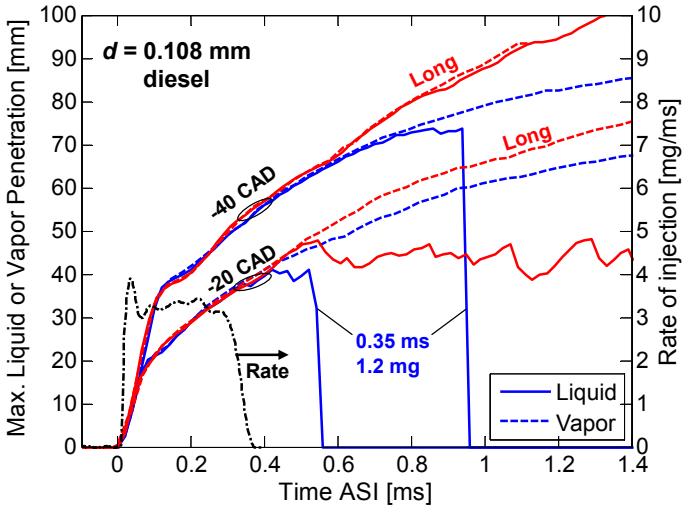

Figure 14. Effect of short injection duration on vapor and liquid penetration as in Fig. 13. Ambient conditions: -20 CAD simulation, 767 K, 10.5 kg/m^3. Injector conditions: 0.108 mm nozzle, 110 MPa, #2 diesel, 1.2 mg injected.

reaches 85 mm by 1.4 ms ASI. Meanwhile, the vapor and liquid phases continue to penetrate and impinge upon the wall (100 mm) at 1.3 ms ASI for the long injection.

These results indicate that the maximum liquid penetration decreased at least 25 mm by resorting to a short injection duration for the -40 CAD condition. However, the Mie-scatter images themselves show that the high-intensity, dense zones of liquid are farther upstream than this. For example, the bright saturated regions of these images penetrate to only about 60 mm at 0.6 ms ASI, a large reduction compared to the long injection. In terms of preventing significant wall-wetting, shortening the injection duration may therefore provide additional benefits even if a small amount of liquid reaches the wall. In general, we believe that our measurement of the maximum liquid penetration is conservative as an indicator for avoidance of practical wall wetting, because the final liquid concentrations in the Mie-scatter images appear quite low. This perspective is consistent with engine experiments and liquid spray visualization in Ref. [7], where some liquid impingement upon the piston bowl and crown were shown, but appeared to have no direct impact on emissions.

We now discuss the liquid and vapor penetration for the -20 CAD condition with the same 0.35-ms injection duration. Results for this condition are shown in the right of Fig. 13 and in the penetration plots of Fig. 14. The initial development of this fuel spray is slower than the -40 CAD condition, because of higher ambient gas density. Fuel penetrates to the head of the jet initially but is then confined to the center of the jet shortly AEI, as shown by a clear vapor boundary on the outside of the jet at 0.4 ms ASI. The liquid evaporates in approximately 0.2 ms AEI for the -20 CAD condition, compared to 0.6 ms AEI for the -40 CAD condition, indicating much faster vaporization. Similar to the -40 CAD result, the vapor boundary continues to penetrate after the liquid is entirely vaporized and the penetration rate is lower than the vapor penetration rate of the long, steady injection.

Although a short injection is used at this -20 CAD condition, the maximum liquid penetration distance almost reaches the quasi-steady liquid length near 40 mm. The fluctuations in the steady liquid length even fall lower than 40 mm during some periods of injection (*e.g.*, 1.1 ms). The benefit in reducing liquid length is therefore marginal at the -20 CAD condition compared to the -40 CAD condition.

One reason that shortening injection duration does not change the liquid penetration as much for the -20 CAD condition is that the time to establish a steady liquid length, t_{ss}, is already quite short, less than 0.6 ms ASI. As shown earlier (Fig. 5), the t_{ss} is less because of the higher ambient gas temperature and density. Since the end of injection occurs only about 0.2 ms prior to t_{ss}, there is less opportunity to limit the maximum liquid penetration.

Effect of Injection Duration or Injection Mass- Figure 15 shows the liquid penetration time history as the injection duration, or the injection mass, is increased. The experimental conditions are the 0.185 mm injector nozzle, using diesel fuel, at the simulated -20 CAD condition. The lower part of the figure indicates that the maximum liquid penetration distance rapidly increases as the injection duration is increased. For another perspective on the effect of injection mass (or duration), the maximum liquid distances during the entire injection period from Fig. 15 are plotted versus the injection mass in Fig. 16. Figure 16 also shows the maximum and minimum in liquid penetration during the steady period, indicating when the short-injection liquid penetrates to the quasi-steady liquid length with statistical significance. These figures show that liquid reaches the steady liquid length using an injection mass of 2.8 mg, a duration of 0.38 ms. Thereafter, an increase in injection duration does not increase the liquid penetration distance because the quasi-steady liquid length is attained, and this length, by definition, does not depend upon the injection duration.

Although liquid reaches the liquid length, the top of Fig. 15 shows that the intensity of the Mie-scatter near the liquid length depends upon the injection duration. Consistent with the discussion about Fig. 13, the liquid density appears much lower for transitional injection durations that just reach the liquid length. The Mie-scatter images at the top of Fig. 15 are at the same time ASI, but the 0.38-ms injection duration has lower intensity than the 0.50-ms injection duration. The transitional injection duration, where the liquid just reaches the liquid length (0.38-ms), may not necessarily mean that there would be significant wall wetting and film formation in an engine in this liquid-length region. More mass could likely be injected without overly

problematic wall-wetting, particularly if the liquid strikes a hot piston.

Nevertheless, decreasing the liquid penetration length by using a short injection may be one of the reasons that early-injection LTC is more successful at low-load conditions compared to high-load conditions. For example, the liquid penetration distances shown in Figs. 15-16 suggest that liquid wall impingement would be substantially reduced, or eliminated in an engine if injecting less than approximately 3 mg at these early-injection CAD. For reference, if an 8-hole nozzle were used in a 2 L/cylinder displacement heavy-duty engine, injecting 3.0 mg/hole, an IMEP of approximately 2.3 bar could be obtained, assuming fuel burns efficiently to completion (*e.g.*, a specific fuel consumption of 200 g / (kw hr)). This is consistent with engine studies that show low-load conditions (<3 bar) typically achieve efficient LTC operation (*e.g.* [6]).

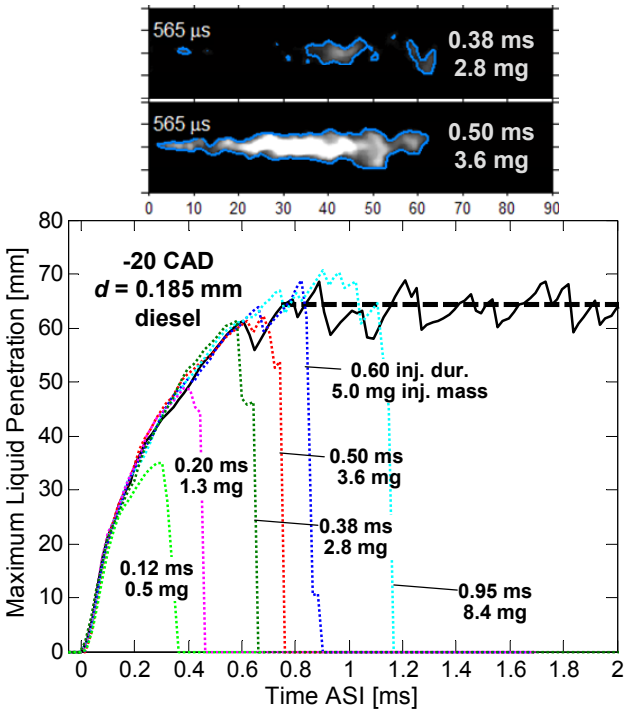

Figure 15. Effect of increasing injection duration on liquid penetration at -20 CAD simulated ambient conditions. Bottom plot shows liquid penetration distances. Top images are Mie-scatter plots for two injection durations when the liquid just reaches the liquid length. Injector conditions: 0.185 mm nozzle, 110 MPa, #2 diesel.

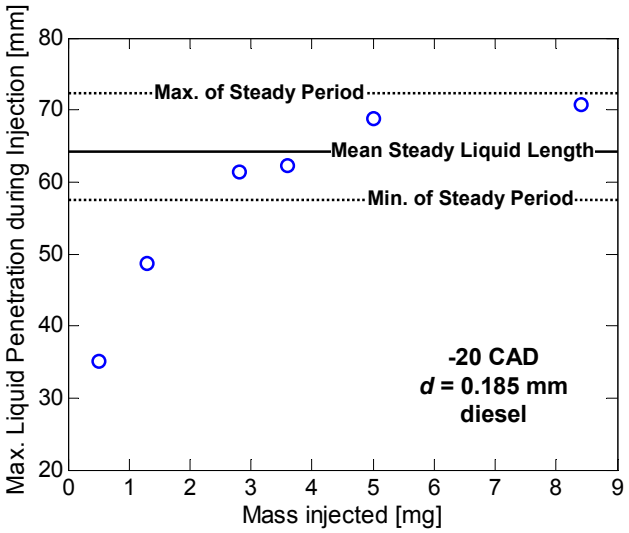

Figure 16. The maximum liquid penetration distance during injection from Fig. 15, plotted against injection mass. The quasi-steady liquid length and maximum and minimum for the quasi-steady period are also shown.

Noting the importance of the actual liquid concentrations that penetrate downstream of the injector, we will continue to use the maximum liquid distance as a conservative metric for limiting liquid penetration by using short injections. In Fig. 17, we show the maximum liquid distance during any period of injection, normalized by the quasi-steady liquid length, and plot this against the injection duration time, normalized by the time (t_{ss}) that long-injection sprays require to reach a quasi-steady liquid length. Experimental data points from many different injector and ambient gas conditions are shown in the figure. When plotted in these normalized coordinates, Fig. 17 shows that there is a general collapse of data.

A major finding shown by Fig. 17 is that it is necessary to make the injection duration (dt_{inject}) approximately 50% of t_{ss}, or less, in order to achieve liquid penetration distances that are lower than the steady liquid length. Clearly, some delay after the end of injection (AEI) is needed for the end of injection "effect" to be "transmitted" to the liquid near the head of the jet, which explains why the injection duration cannot be close to t_{ss}. Alternatively, if the time AEI for mixing information to reach the head of the jet (to decease liquid penetration) was equal to t_{ss}, the ratio of injection duration to t_{ss} would necessarily be lower than 0.50, in contrast to our results. However, current research on the jet mixing processes

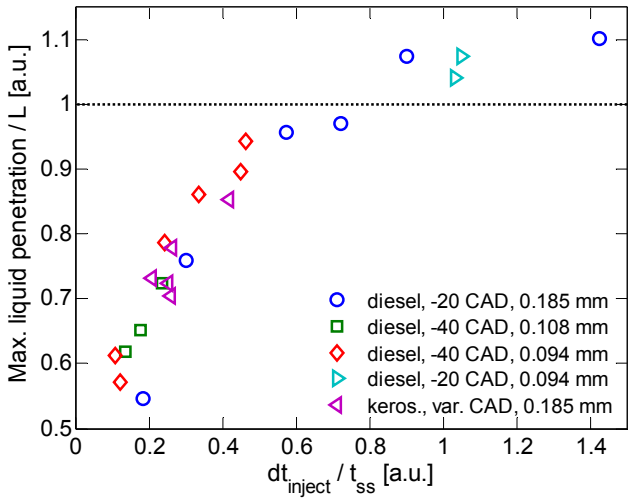

Figure 17. Effect of injection duration on liquid penetration. Injection duration is normalized by the time for a spray to reach a steady liquid length at a given condition. The maximum liquid penetration during injection is normalized by the steady liquid length. Various experimental conditions are given in the legend..

that occur AEI shows that an "entrainment wave", indicative of enhanced relative fuel-ambient mixing, travels from the injector approximately twice as fast as the initial jet penetration rate [33]. Consequently, increased mixing AEI is expected to affect the head of the jet in only one-half of the time that it took for a steady jet to penetrate to that location. As a result, the entrainment wave reaches the head of the jet at double the injection duration of a finite injection [33]. This is essentially the dt_{inject} / t_{ss} = 0.5 condition given in Fig. 17.

Evidence of the entrainment wave reaching the head of the jet at double the injection duration time can actually be observed in the vapor penetration curves given in Fig. 14. For example, the -40 CAD condition shows that the vapor penetration for the short injection begins to depart from the penetration of the long injection after about 0.6 ms, which is a factor of two greater than the time of ramp-down in the rate of injection profile. A slower penetration occurs when the momentum deficit associated with the end of injection reaches the head of the jet through this entrainment wave, causing velocities to fall below those of the steady jet.

For liquid penetration, rather than vapor penetration, the penetration distance of interest is the steady liquid length (L). As was shown in Fig. 2, the vapor and liquid penetrate at the same rate until reaching L. Therefore, t_{ss} is driven by the penetration rate of a long injection spray. For short injection sprays, the liquid penetration follows that of a long injection spray during the time of injection (see Fig. 14). After the end of injection, enhanced mixing is needed to prevent liquid from reaching the steady liquid length. If liquid does not reach L, we presume that mixing with the ambient has been increased at the jet head, prior to jet head reaching L, as appears obvious from the images shown in Fig. 13. An entrainment wave that reaches the head of the jet at a time double the injection duration will therefore tend to decrease the liquid penetration, in agreement with the results given in Fig. 17.

Constant Mass Injection using Different Techniques- With the need to inject more fuel to reach higher-load LTC, while avoiding liquid penetration to the quasi-steady liquid length, we ask what is the optimal injector nozzle size and injection pressure to achieve this goal? As has already been shown, reducing the nozzle size will reduce the steady liquid length. However, one must inject fuel for a longer duration to inject the same mass, and this will increase the liquid penetration distance until reaching the steady liquid length. Therefore, when transients of injection are considered, it is not clear that a small nozzle size is preferred to limit liquid penetration. To examine this tradeoff, we left the injection mass constant, by decreasing either the nozzle diameter or injection pressure and increasing the injection duration.

Figure 18 shows the liquid penetration and rate of injection for three different nozzle diameters, injecting 1.3 mg total mass in each case at -40 CAD simulated conditions. The liquid penetration rate decreases with decreasing nozzle size, but, remarkably, the maximum liquid penetration is approximately the same, at about 80 mm. This distance remains less than the steady-state liquid length for each nozzle (the lowest steady liquid length is shown for the 0.094 mm nozzle on the figure). These results suggest that liquid penetration may be independent of nozzle size, provided the same total mass of fuel is injected and the maximum liquid penetration distance is lower than the steady-state liquid length.

To consider this hypothesis further, we left the nozzle size fixed and varied the injection pressure. Much like a smaller nozzle diameter, a lower injection pressure requires a longer injection duration to deliver the same total mass. The result is shown in Fig. 19 for three different injection pressures, at both -40 CAD, and -20 CAD simulated conditions. Once again, the maximum

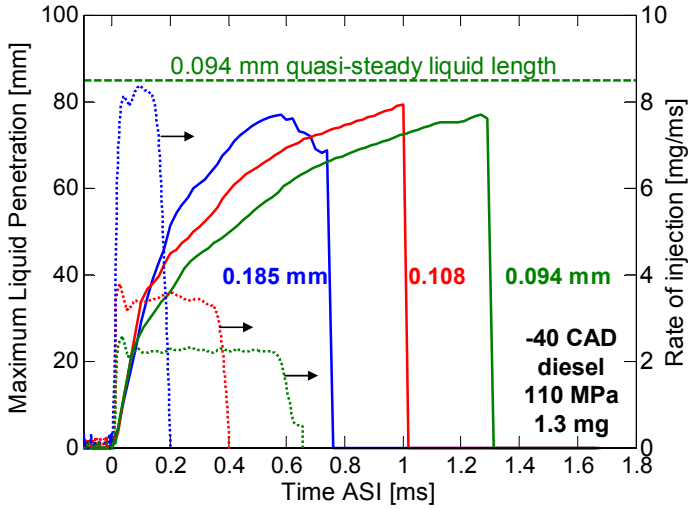

Figure 18. Liquid penetration distance with 1.3 mg injection for various nozzle sizes. Rate of injection at right. Simulated ambient conditions of -40 CAD (Fig. 1) Injector conditions: 110 MPa, diesel.

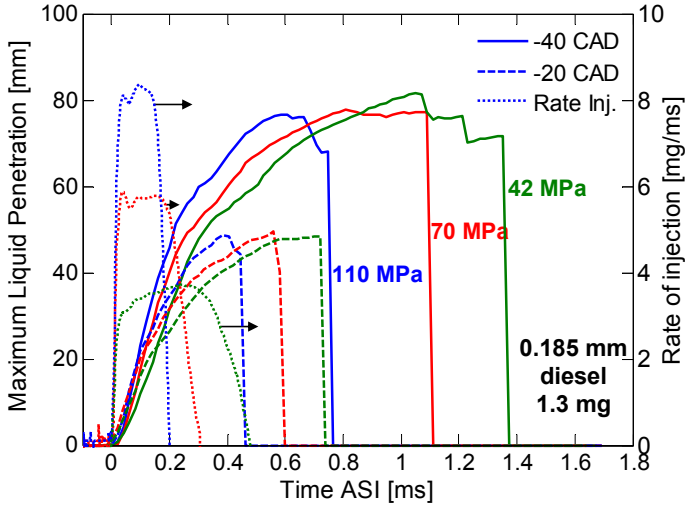

Figure 19. Effect of injection pressure variation on liquid penetration, with 1.3 mg mass injected. -40 (solid) and -20 (dashed) CAD simulated ambient conditions. Injector conditions: 0.185 mm nozzle, #2 diesel.

liquid penetration appears to depend only on the injected mass, rather than injection pressure, for a given CAD condition. The low-pressure sprays penetrate more slowly, as expected, but the final liquid penetration distance is the same.

An important difference between Fig. 18 and Fig. 19 is that the steady-state liquid length does not depend upon injection pressure, which is not true for nozzle diameter (see Table 1). Of course, the steady liquid length depends upon the particular CAD, but the maximum liquid penetration in Fig. 19 remains less than the steady-state liquid length for the two CAD shown (wall impingement at -40 CAD and 65 mm (see Fig. 16) at -20 CAD).

Figure 20 shows the maximum liquid penetration when nozzle diameter is varied, at an earlier CAD of -20 CAD, while again maintaining the same 1.3 mg injection mass. For reference, the transient liquid penetration for a long, steady injection is also given on the figure. With injection timing closer to TDC, the maximum liquid penetration increases with increasing nozzle diameter, even though the injection mass is the same, and only 1.3 mg. However, at this -20 CAD condition, the liquid penetration appears to have reached the steady liquid length for both the 0.108 mm and 0.094 nozzles. Since steady liquid lengths depend upon nozzle diameter, it is therefore not surprising that the maximum liquid distance is no longer independent of nozzle diameter, as it was for the -40 CAD condition shown in Fig. 18. Note that the maximum liquid penetration is different despite the fact that the 0.185 mm liquid penetration is far lower than its steady liquid length.

These results show that the dependence of maximum liquid penetration distance upon injection mass, rather than injection pressure or nozzle diameter, is valid only if the CAD timing and mass injected produces transient liquid lengths that are less than the quasi-steady liquid length. In this sense, knowledge of the quasi-steady liquid length as a function of CAD is important at early injection conditions, in order to optimize the CAD timings and injection hardware for short injection events that have the greatest potential to reduce liquid penetration.

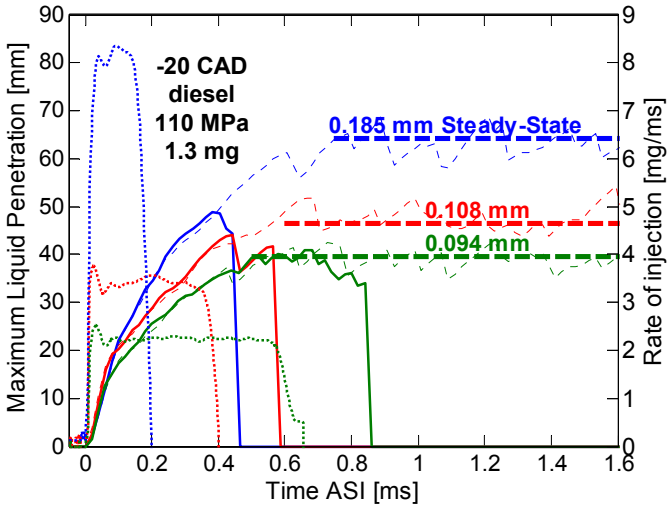

Figure 20. Liquid penetration for three different nozzle sizes with -20 CAD simulated conditions. Compare to Fig 18.

Effects of Injection Duration and Engine Phasing- For an engine, the timing of spray development will ultimately affect the maximum liquid distance, in addition to the effect of injection duration. For example, injection pressure variation does not change the steady liquid length at a given CAD timing, as shown above for constant-volume conditions, but the timing of maximum liquid penetration is delayed when injection pressure is low. In a running engine, compression increases the ambient gas temperature and density with increasing time, thereby providing energy to vaporize the fuel. Therefore, the liquid penetration would be expected to be less when using a low injection pressure and a short transient injection, provided the start of injection is the same.

To illustrate the potential effect of compression heating on liquid penetration with different injection pressures, we have fit the measured quasi-steady liquid lengths as a function of CAD (Fig. 8), and then converted CAD to time ASI, assuming an engine speed of 1800 rpm. Normalizing the liquid length *versus* time by the value at -40 CAD, we obtain a scale factor that decreases from unity with increasing time, starting at -40 CAD. We use the original data shown in Fig. 19 and multiply it by this scale factor as an example of how compression heating can reduce the transient liquid penetration. The result is now plotted in Fig. 21. This exercise is not meant to be quantitative for an actual spray during compression, but is simply used schematically to demonstrate a major effect of compression.

The significant point of Fig. 21 is that compression-heating reduces the liquid penetration more for sprays that take more time to develop. Therefore, in a real

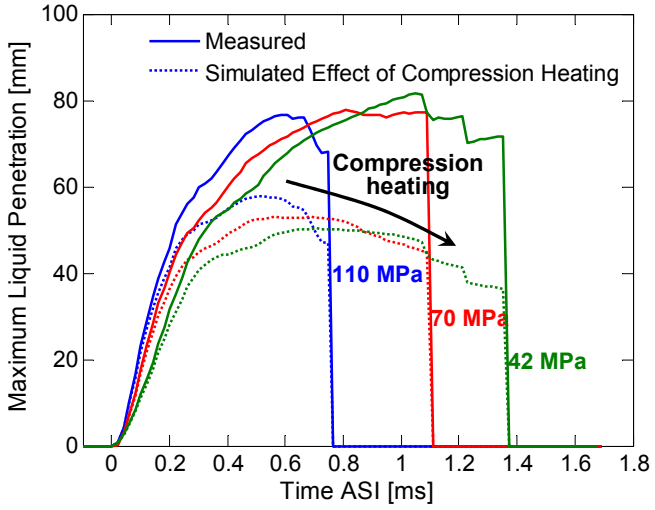

Figure 21. Effect of compression-heating on liquid penetration, illustrated using -40 CAD data from Fig. 19.

engine, low-injection pressure, or small-nozzle early injections (of the same mass) are expected to have lower liquid penetration than their counterparts. However, the fact that the injection duration for these sprays is longer may work against the LTC goals of producing a well-mixed charge, since there is less ignition dwell (time from end of injection to ignition). The experimental observation that these sprays are the last to vaporize, by itself, suggests that the mixture is more fuel rich at a given time ASI. Although the liquid penetration should be less for sprays that develop more slowly (again assuming the same start of injection), this tradeoff must be considered for LTC engines.

MULTIPLE INJECTIONS TO LIMIT LIQUID PENETRATION- The last section demonstrated that short injections can limit liquid penetration, but the mass per injection must be minimized to prevent the liquid from reaching the steady-state liquid length. Potentially, short, multiple injections could be used to add more fuel mass, while still limiting the liquid penetration. Indeed, some researchers have shown that liquid wall impingement is reduced when using multiple injections in an engine [8]. We investigate the effect of multiple injections on liquid penetration in this section.

Attempting to minimize liquid penetration, while also injecting the fuel as early as possible, we examined multiple injection scenarios with short injections, and also minimal dwell between injections. Through trial and error we varied the electronic controls for the injector to produce a four-injection event with the injection duration and dwell as close as possible for each injection. Figure 22 shows the liquid and vapor penetration for a four-injection event. Similar to Fig. 13, the top of Fig. 22 shows combined shadowgraph and Mie-scatter boundaries representing the vapor and liquid phases, respectively. The vapor and liquid penetration distances, as well as rate of injection, are plotted at the bottom, and compared to those of a long injection duration. The injection duration for each injection was approximately 0.2 ms and there is about 0.3 ms dwell between injections, which is near the limit of the injector capability. Results are provided for the -40 CAD condition, using diesel fuel and the 0.108 mm nozzle. This condition has a steady-state liquid length that reaches the wall of the chamber (100 mm) as shown by the long injection curve.

The shadowgraph/liquid images show the penetration and vaporization of the first injection up until 0.4 ms ASI. Similar to that shown in Fig. 13, the vapor and liquid penetrate together and, after the end of injection, liquid remains to be vaporized near the jet head. At 0.5 ms, the second injection begins. During this second injection, the liquid remaining from the first injection is visible in front of the penetrating spray at 0.6 ms, as there is a clear break in the liquid regions between these two sprays near 40 mm. Because of the separation in liquid borders, it was possible to extract the initial penetration rate of the second injection until the two liquid zones merged. The

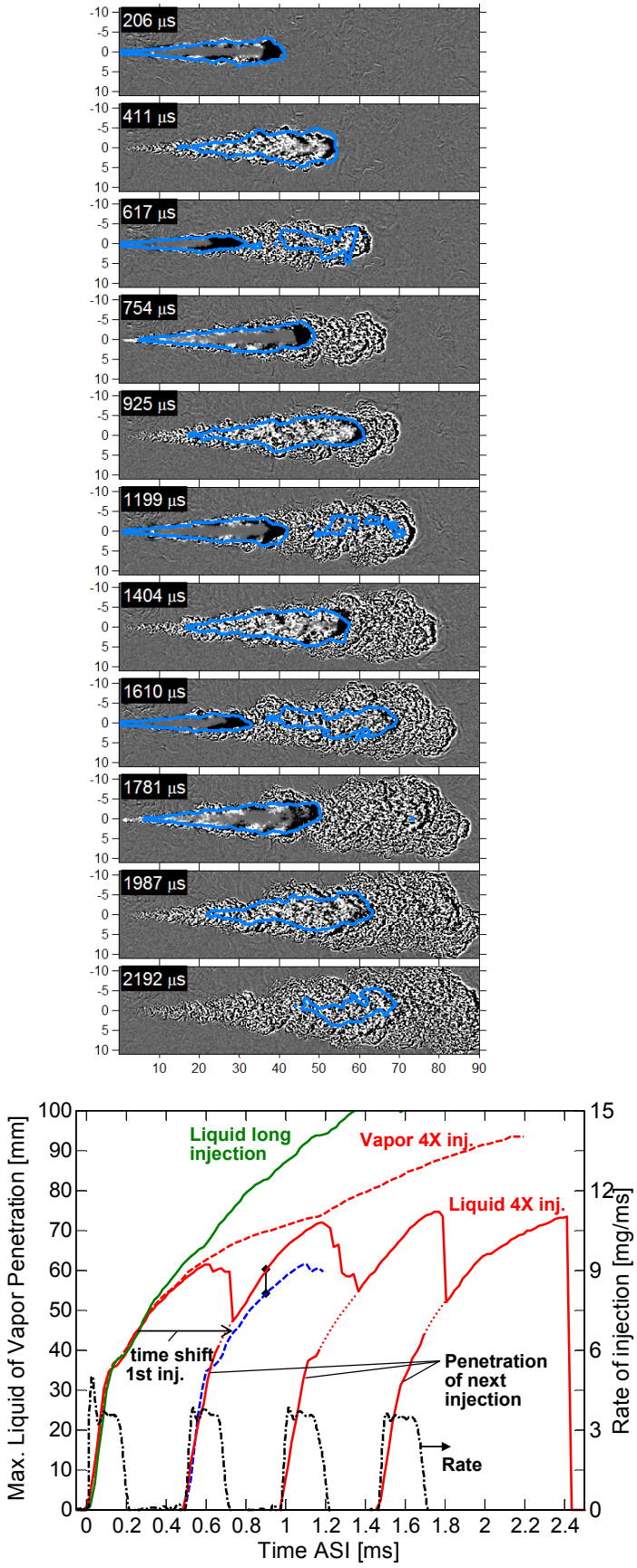

Figure 22. Effect of multiple injections on vapor and liquid penetration. (top) shadow/Mie-scatter images. (bottom) Penetration and injection rate. Compare to long injection at the same conditions. Ambient conditions: -40 CAD simulation, 600 K, 5.2 kg/m^3. Injector conditions: 0.108 mm nozzle, 110 MPa, #2 diesel, approximately 2.8 mg injected. Image scale in mm.

value of liquid penetration of the second and following injections is therefore shown in the figure with dotted lines showing the time when the liquid borders have merged.

At 0.75 ms the liquid from the first injection has vaporized completely and the second injection is penetrating within the vapor region left from the first injection. In the figure, the penetration profile of the first injection has been shifted in time (dashed blue curve) to have the same start of injection as the second injection. It is clear that the second injection penetrates more quickly than the first injection. For example, the liquid penetration at 0.9 ms is approximately 0.4 ms after the start of the second injection, which matches the time ASI of the second image down. Although the time ASI matches, the penetration of the second injection has reached 60 mm, compared to only 55 mm for the first injection. This difference in penetration is highlighted in the penetration distance plot with an arrow at 0.9 ms. Here, the liquid penetration rate of the second injection is shown to be slightly less than that of the first injection, at least initially. This lower penetration rate is possibly caused by a slower ramp-up in the rate of injection for the second injection, as indicated in Fig. 22. Despite this, the second injection overtakes the first injection and eventually penetrates farther than the first injection.

The differences in penetration rate appear to be the largest after the end of the second injection. The maximum liquid penetration of the first injection was only 60 mm, but the second injection penetrates to about 70 mm, nearly reaching the vapor boundary remaining from the first injection. Liquid from subsequent third and fourth injections also penetrates farther than the first injection, but the final penetration distance is not significantly different than the second injection. Although the injector duty cycle appears to have produced a maximum liquid penetration distance of about 70 mm, the vapor phase of the spray continues to penetrate downstream.

This multiple injection strategy is clearly helpful in reducing liquid penetration as the final 70-mm penetration distance remains much less than the steady-state liquid length. Indeed, if these injections are combined together into a single injection (0.8 ms duration), the liquid penetration follows the same path denoted by the “long” injection, touching the vessel wall at 100 mm. Still, it is interesting that liquid from the subsequent injections penetrates farther than that of the first injection.

There are two factors that likely contribute to this behavior. First, the penetration rate of the second injection can be higher than the first injection because the second enters into a “wake” region left by the first. A frame-by-frame shadowgraph visualization confirms that fluid (vapor) is moving downstream in front of the second liquid injection. In contrast, the first injection encounters stagnant fluid that it must push away. Therefore the first injection penetration rate is less than the second injection. In-cylinder flow fields, such as a strong swirl, may have some effect on these results, since our chamber is essentially quiescent. However, even when using swirl, the low ambient gas density for an early-injection condition will not deflect the spray as much as that at TDC injection. Consequently, the potential for spray dominated mixing, and interaction between injections, remains high when employing multiple injections at early-injection conditions.

A second reason that liquid from subsequent injections penetrates farther than the first injection is that mixing of the second injection takes place with a cooler, vaporized fuel-ambient mixture. The shadowgraph sequence shows that liquid boundaries for the second or later injections remain within the vapor boundary of the former injection. Frame-by-frame analysis even shows vapor structures at the edge of the jet that are re-entrained into the jet as the next fast-moving spray moves through the mixture. As a consequence of mixing with a fuel-laden, cool ambient, it would be more difficult for the second injection to reach temperatures that are high enough, and mixtures that are fuel-lean enough, for complete vaporization. The maximum liquid penetration therefore increases.

A countering effect potentially produced by the first injection that could decrease the liquid penetration of the second injection is that the first injection enhances turbulence. In particular, recent work shows that there is a strong enhancement of entrainment after the end of injection [32,33]. However, the same measurements show that fuel-lean mixtures persist near the injector for some time after the end of injection and that these mixtures quickly stagnate [32]. Therefore, if turbulence is enhanced by the first injection, the turbulence quickly decays such that it cannot overcome the other factors discussed above to reduce the liquid penetration. Also, recall that the dwell between injections was minimized for this injector, and so the potential for effects of any enhanced turbulence from the previous injection is already maximized for this injector configuration.

Similar to the discussion about the effect of prolonging injection duration, using smaller nozzle diameters or lower injection pressure, we note that compression-heating would tend to reduce the liquid penetration for injection events that occur closer to TDC in an engine. For example, the last injection starts at 1.5 ms ASI in Fig. 22, a time that corresponds to 15 CAD at 1800 rpm. As compression for 15 CAD would significantly reduce the liquid penetration, this last injection would likely not have higher liquid penetration than the first injection, despite the results given here in the constant-volume chamber. On the other hand, the fuel delivery of multiple injections may not necessarily produce optimal LTC combustion. Earlier injections may begin to ignite, preventing the later injections from mixing and achieving less fuel-rich combustion. Although the principle of multiple injections works to reduce the liquid penetration,

possibly preventing wall wetting, these additional factors must be considered for successful LTC in an engine.

CONCLUSIONS

Early-injection LTC strategies permit the spray to penetrate into a low ambient temperature and density environment where vaporization is poor and liquid impingement upon the cylinder liner and piston bowl are more likely to occur. The liquid penetration of diesel sprays was studied at these early-injection conditions in an optically accessible chamber with a free path of 100 mm, the large geometry minimizing effects of wall interaction and liquid impingement. The chamber also allowed assessment of spray penetration at well-controlled ambient gas temperature and density conditions that were constant during injection. High-speed Mie scatter imaging was chosen to resolve the liquid spray penetration transients and to identify the time and distance of an established quasi-steady liquid length. The effects of nozzle diameter, injection pressure, intake boost (ambient density), fuel type, injection duration, and multiple injections, were all considered.

Conclusions from this study can be summarized as follows:

- The crank angle timing of injection strongly affects the maximum liquid penetration, as determined by the increased charge gas temperature and density. For #2 diesel fuel and a 0.108 mm nozzle, the steady liquid length decreases from 88 mm at -35 CAD to 47 mm at -20 CAD, a reduction of nearly a factor of two.

- Although the liquid penetration length is longer for earlier CAD timing, the jet development time to reach this steady liquid length is also longer. Understanding the time that a spray reaches the steady liquid length is important because of transient events (compression, etc.) occurring in-cylinder.

- Increased intake pressure (boost) shortens the steady liquid penetration, possibly preventing wall impingement. The time to reach a steady liquid length depends upon the particular CAD temperature. At 600 K, the time to reach increases with increasing ambient density, while at 767 K, the opposite is true.

- Decreasing the injection duration to approximately one-half of the time that a spray attains quasi-steady liquid penetration can lower the maximum penetration distance for the transient injection, potentially avoiding wall wetting. A small injection duration ultimately limits the amount of mass injected, however, which may be one contributing reason that LTC engines perform better at low-load conditions.

- Small nozzle diameters are helpful in limiting liquid penetration if sprays reach a steady-state liquid length. However, if the injection mass is kept constant, requiring a longer injection duration with small nozzles, the same maximum liquid penetration results as that of larger nozzles. This result is true only if the injection durations are short enough such that liquid does not reach the steady-state liquid length.

- Similar to the nozzle diameter findings, the maximum liquid penetration for short-injection events at different injection pressure depends upon only the injected mass. That is, short injection durations at high injection pressure produce the same maximum liquid penetration as longer injection durations at low injection pressure.

- Multiple injections limit the liquid penetration to be less than that of a steady-state spray, when the injection events are short. For equally spaced injections and dwell between injections, the liquid penetration from the second injection is longer than the first injection. The second injection penetrates farther than because the first injection leaves a cool, fuel-laden mixture in its wake.

- A kerosene fuel, with lower boiling point than #2 diesel, shows an expected benefit of a shorter quasi-steady liquid length, making this lighter, more volatile fuel more resistant to wall-wetting. Kerosene is also more tolerant to early injection timing as the comparative change in liquid length is less than that of diesel. The time to reach a steady-state liquid length, and the time to vaporize after the end of injection, are also less for kerosene compared to diesel.

ACKNOWLEDGMENTS

Support for this research was provided by the DOE Office of Vehicle Technologies. The kerosene fuel sample was gratefully provided by Chevron Energy Technology Company. The research was performed at the Combustion Research Facility, Sandia National Laboratories, Livermore, California. Sandia is a multiprogram laboratory operated by Sandia Corporation, a Lockheed Martin Company, for the United States Department of Energy's National Nuclear Security Administration under contract DE-AC04-94AL85000. The authors thank Dave Cicone of Sandia National Laboratories for assistance in the laboratory.

REFERENCES

1. Zhao, F. Asmus, T.N., Assanis, D., Najt, P.M., Dec, J.E., Eng, J.A. Homogeneous charge compression ignition (HCCI) engines - key research and

development issues, Society of Automotive Engineers, Warrendale, PA. SAE, 2003.
2. Kanda, T., Hakozaki, T., Uchimoto, T., Hatano, J., Kitayama, N., and Sono, H., "PCCI Operation with Early Injection of Conventional Diesel Fuel," SAE Paper 2005-01-0378, SAE Transactions, 114, No. 3, pp. 584-593, 2005.
3. Klingbeil, A. E., Juneja, H., Ra, R., and Reitz, R. D., "Premixed Diesel Combustion Analysis in a Heavy-Duty Diesel Engine," SAE Paper 2003-01-0341, SAE Transactions, 112, 2003.
4. Musculus, M. P. B., "Multiple Simultaneous Optical Diagnostic Imaging of Early-Injection Low-Temperature Combustion in a Heavy-Duty Diesel Engine," SAE Paper 2006-01-0079, SAE Transactions, 115, No. 3, pp. 83-110, 2006.
5. Hardy, W. L. and Reitz, R. D., "A Study of the Effect of High EGR, High Equivalence Ratio, and Mixing Time on Emissions Levels in a Heavy-Duty Diesel Engine for PCCI Combustion," SAE Paper 2006-01-0026, 2006.
6. Kook, S., Bae, C., Miles, P. C., Choi, D., and Pickett, L. M., "The Influence of Charge Dilution and Injection Timing on Low-Temperature Diesel Combustion and Emissions," SAE Paper 2005-01-3837, SAE Transactions, 114, No. 4, pp. 1575-1595, 2006.
7. Kook, S., Bae, C., Miles, P. C., Choi, D., Bergin, M., and Reitz, R. D., "The Effect of Swirl Ratio and Fuel Injection Parameters on CO Emission and Fuel Conversion Efficiency for High-Dilution, Low-Temperature Combustion in an Automotive Diesel Engine," SAE Paper 2006-01-0197, 2006, SAE Transactions, 115, No. 3, pp. 111-132, 2007
8. Hotta, Y., Inayoshi, M., Nakakita, K., Fujiwara, K., and Sakata, I., "Achieving Lower Exhaust Emissions and Better Performance in an HSDI Diesel Engine With Multiple Injection," SAE Paper 2005-01-0928, SAE Transactions, 114(3), 2005.
9. Opat, R., Ra, Y., Gonzalez, M. A., Krieger, R., Reitz, R. D., Foster, D. E., Durret, R. P., and Siewert, R. M., "Investigation of Mixing and Temperature Effects on HC/CO Emissions for Highly Dilute Low Temperature Combustion in a Light-Duty Diesel Engine," SAE Paper 2007-01-0193, 2007.
10. Minato, A., Tanaka, T., and Nishimura, T., "Investigation of Premixed Lean Diesel Combustion with Ultra High Pressure Injection," SAE Paper 2005-01-0914, SAE Transactions, 114, No. 3, pp. 756-764, 2005.
11. Walter, B. and Gatellier, B., "Development of the High Power NADI Concept Using Dual Mode Diesel Combustion to Achieve Zero NOx and Particulate Emissions," SAE Paper 2002-01-1744, SAE Transactions, 111, No. 4, pp. 779-787, 2002.
12. Lechner, G. A., Jacobs, T. J., Chryssakis, C. A., Assanis, D., and Siewert, R. M., "Evaluation of a Narrow Spray Cone Angle, Advanced Injection Timing Strategy to Achieve Partially Premixed Compression Ignition Combustion in a Diesel Engine," SAE Paper 2005-01-0167, 2005.
13. Siewert, R. M., "Spray Angle and Rail Pressure Study for Low NOx Diesel Combustion," SAE Paper 2007-01-0122, 2007.
14. Kashdan, J., Mendez, S., and Bruneaux, G., “On the Origin of Unburned Hydrocarbon Emissions In a Wall Guided, Low NOx Diesel Combustion System”, JSAE Paper 20077038; also in SAE 2007-01-1836, 2007.
15. Fang, T., Coverdill, R. E., Lee C.F., and White, R. A., "Smokeless Combustion Within a Small-Bore HSDI Diesel Engine Using a Narrow Angle Injector," SAE Paper 2007-01-0203, 2007.
16. Martin, G. C., Gehrke, C., Mueller, C. J., Radovanovic, M., and Milam, D., "Early Direct-Injection, Low-Temperature Combustion of Diesel Fuel in an Optical Engine Utilizing a 15-Hole, Dual-Row, Narrow-Included-Angle Nozzle," SAE Paper 2008-01-2400, 2008.
17. Yokota, H., Kudo, Y., Nakajima, H., Kakegawa, T., and Suzuki, T., "A New Concept for Low Emission Diesel Combustion," SAE Paper 970891, 1997.
18. Cursente, V., Pacaud, P., Mendez, S., Knop, P., and de Francqueville, L., "System Approach for Compliance With Full Load Targets on a Wall Guided Diesel Combustion System," SAE Paper 2008-01-0840, 2008.
19. Kalghatgi, G. T., Risberg, P., and Angstrom, H.-E., "Advantages of Fuels With High Resistance to Autoignition in Late-Injection, Low-Temperature, Compression Ignition Combustion," SAE Paper 2006-01-3385, 2006.
20. Bessonette, P. W., Schleyer, C. H., Duffy, K. P., Hardy, W. L., and Liechty, M. P., "Effects of Fuel Property Changes on Heavy-Duty HCCI Combustion," SAE Paper 2007-01-0191, 2007.
21. Siebers, D.L., “Liquid-Phase Fuel Penetration in Diesel Sprays,” SAE Paper 980809, 1998.
22. Siebers, D.L. “Scaling Liquid-Phase Fuel Penetration in Diesel Sprays Based on Mixing-Limited Vaporization.” SAE Paper 1999-01-0528, 1999.
23. Espey, C. and Dec, J. E., "The Effect of TDC Temperature and Density on the Liquid-Phase Fuel Penetration in a D.I. Diesel Engine," SAE Paper 952456, SAE Transactions, 104(4):1400-1416, 1995.
24. Alfuso, S., Allocca, L., Auriemma, M., Caputo, G., Corcione, F. E., Montanaro, A., and Valentino, G., "Analysis of a High Pressure Diesel Spray at High Pressure and Temperature Environment Conditions," SAE Paper 2005-01-1239, 2005.
25. Desantes, J. M., Pastor, J. V., Payri, R., and Pastor, J. M., "Experimental Characterization of Internal Nozzle Flow and Diesel Spray Behavior. Part II: Evaporative Conditions," Atomization and Sprays, 15:517-543, 2005.

26. Naber, J. D. and Siebers, D. L., "Effects of Gas Density and Vaporization on Penetration and Dispersion of Diesel Sprays," SAE Paper 960034, SAE Transactions, 105(3):82-111, 1996.
27. Engine Combustion Network experimental data archive, http://www.ca.sandia.gov/ECN/.
28. Siebers, D., Higgins, B., and Pickett, L. M., "Flame Lift-Off on Direct-Injection Diesel Fuel Jets: Oxygen Concentration Effects," SAE Paper 2002-01-0890, SAE Transactions, 111(3):1490-1509, 2002.
29. Kook S., Pickett, L.M., Musculus, M.P.B., and Gemlich, R.K., “Influence of Diesel Injection Parameters on End-of-Injection Liquid Length Recession”, SAE Paper 09-PFL-1079, 2009.
30. Settles. G. S., *Schlieren and Shadowgraph Techniques*, Springer-Verlag, 2001.
31. Pickett, L. M., Kook, S., and Williams, T. C., "Visualization of Diesel Spray Penetration, Cool-Flame, Ignition, High-Temperature Combustion, and Soot Formation Using High-Speed Imaging," SAE Paper 09PFL-1082, 2009.
32. Musculus, M. P. B., Lachaux, T., Pickett, L. M., and Idicheria, C. A., "End-of-Injection Over-Mixing and Unburned Hydrocarbon Emissions in Low-Temperature-Combustion Diesel Engines," SAE Paper 2007-01-0907, SAE Transactions, 116, 2007.
33. Musculus, M. P. B. and Kattke, K., "Entrainment Waves in Diesel Jets," SAE Paper 09PFL-0538, 2009.

CONTACT

Lyle M. Pickett: LMPicke@sandia.gov

S. Hoon Kook: skook@sandia.gov